ORNL/SPR-2020/1565

Summary of the Postirradiation Examination of the First Samples from a MiniFuel Irradiation

Nuclear Technology Research and Development

Prepared for
US Department of Energy
Advanced Fuels Campaign
J.M. Harp, R.N. Morris, C.M. Petrie,
J.R. Burns, D.J. Skitt, K.A. Terrani
Oak Ridge National Laboratory
June 12, 2020
M2FT-20OR020201071

ABSTRACT

An overview of postirradiation examination results for uranium nitride kernels and uranium nitride coated particles irradiated in the High Flux Isotope Reactor are presented. This is the first postirradiation examination of the MiniFuel irradiation vehicle that was recently developed to rapidly screen different nuclear fuel concepts. Observations on fission gas release, irradiation conditions, and microstructure of the irradiated fuel show good fuel performance at the low burnup achieved in this initial irradiation. The burnup measured by mass spectrometry ranged from 5.9 to 10 MWd/kgU, as was achieved after only 68 effective full power days of irradiation. Results from silicon carbide thermometry measurements further benchmarked the MiniFuel irradiation vehicle and indicated that the fuel was irradiated at temperatures ranging from 410–460°C. Extensive microstructural characterization of the irradiated fuel was performed, and no significant irradiation induced changes were observed.

This page is intentionally left blank.

CONTENTS

This page is intentionally left blank.

FIGURES

SUMMARY OF THE POSTIRRADIATION EXAMINATION OF THE FIRST SAMPLES FROM A MINIFUEL IRRADIATION

1. INTRODUCTION

Historically, novel nuclear fuel concepts, and even incremental changes to established nuclear fuel concepts, have been evaluated by iteratively irradiating fuels in prototypic fuel geometries, neutron flux conditions, and temperatures in integral fuel tests that approximated the fuel concept environment. During iterations, conditions were made incrementally more strenuous until fuel failure was observed. This approach has been used to establish the acceptable fuel performance envelope for the fuel concept, and it was successful for several fuel concepts that were evaluated in the first few decades of the nuclear industry, with the UO_2–Zircaloy system used in light water reactors being the best example. However, this approach is inherently slow and expensive, due in part to the long times needed to irradiate fuel to higher and higher fission densities (burnup) and perform postirradiation examinations (PIE) on the resulting experiments. This approach also only established a narrow set of operating conditions in which fuel behavior was well understood. This process is well documented by Crawford et al. [1] and is expected to require decades to complete.

Renewed interest in novel fuel concepts now demands a more nimble approach to irradiation testing. The evaluation of new or minimally studied fuel concepts requires accelerated testing to more quickly screen fuel concepts at several different irradiation conditions while leveraging modeling and simulation capabilities to target the experimental evaluations of key fuel properties that have the greatest impact on fuel performance. The MiniFuel irradiation vehicle is designed to rapidly evaluate nuclear fuel material under well-controlled conditions while minimizing the number of variables that occur during irradiation [2]. In MiniFuel irradiations, heating is de-coupled from fission rate so that concepts can be evaluated under a specific condition—temperature, composition, geometry, etc.—while simultaneously varying other conditions. Additionally, by decoupling the heating, it is possible to rapidly accumulate fission density compared to prototypic condition integral testing. The result is accelerated screening of concepts in the separate-effects stage of testing. Separate-effects tests like those planned for MiniFuel can be used to collect data and develop parameters for models of different irradiation-induced phenomena, or they can be used to confirm existing mechanistic models. This is particularly important in the current modeling efforts, as the highly detailed and computationally intensive investigations focused on first principle calculations require large amounts of data under many different irradiation conditions to achieve the high-fidelity phenomena modeling with the minimum number of empirical parameters. Once well validated, mechanistic models can then be used to predict the behavior of the same fuel concepts in an integral test. This approach to fuel testing increases the efficiency of integral testing at prototypic conditions by both screening out poor fuel concepts and providing foundational data of fuel performance before integral testing is performed.

2. SUMMARY OF IRRADIATION TEST

The design of the MiniFuel irradiation vehicle is documented in the paper by Petrie et al. [2] and is illustrated in Figure 1. In this test, small fuel samples are placed in compatible material cups (Mo in the first MiniFuel irradiations) that are then placed inside a capsule containing a relatively massive high atomic number filler material (again Mo in the initial irradiation). This filler material produces the majority of heat in the capsule through gamma heating rather than fission, and it also contains a silicon carbide (SiC) thermometry sensor. The current design includes 6 capsules inside a single target capsule that is then placed into a basket that locates the experiment in a specific location in the High Flux Isotope

Reactor (HFIR) outer reflector. The thickness and composition of the gas in the gap between the target capsule inner diameter and capsule outer diameter are used to control the temperature of the fuel samples; this gas is typically helium.

The initial fuel evaluated in MiniFuel irradiations is related to the development of UN tristructural isotropic (TRISO) fuel [3]. This fuel form was developed as a high actinide density variation on TRISO fuel, which was developed under the US Department of Energy (DOE) Advanced Gas Reactor program [4–9]. This utilization of nitrides in coated particle nuclear fuel is different from historical applications of nitrides for fast reactors as driver fuel [10,11] or as an actinide destruction targets [12,13]. This irradiation seeks to further investigate the performance of this fuel form to help optimize fuel fabrication parameters for UN TRISO, such as coating layer thickness and coating parameters, which are based on optimized parameters for smaller, less dense uranium oxide / uranium carbide TRISO developed for the Advanced Gas Reactor program. To this end, the irradiated MiniFuel targets contained uranium nitride kernels with 4 different composition variations and a density variant; in addition, they contained kernels with full TRISO coatings. The irradiation matrix is shown in Table 1, and more details about the samples are documented in the literature [14–18].

There were 2 MiniFuel targets designated MF01 and MF02 inserted into HFIR in June 2018 in the VXF-15 irradiation position. See Figure 2 for pre-irradiation photos and x-ray radiography of these targets. The basket used for this irradiation has 3 radial positions and 3 axial positions for each radial position. A target position is specified as *R*-*A*, *R* being the radial position, and *A* the axial position in the basket. Radial positions 2 and 3 face toward the core, and radial position 1 is partially shielded from the core by the other positions. This is illustrated on the left side of Figure 1. The MF01 target had a burnup goal of 1% fissions per initial heavy metal atoms (FIMA) and was in the 2-2 position in the MiniFuel basket. The MF02 target has a burnup goal of 6% FIMA and is located at the 3-2 position in the HFIR basket. Each capsule was numbered from the bottom to the top of the core using the integers 1–6. The positioning of each capsule also served as its identifying mark for PIE (see Table 1).

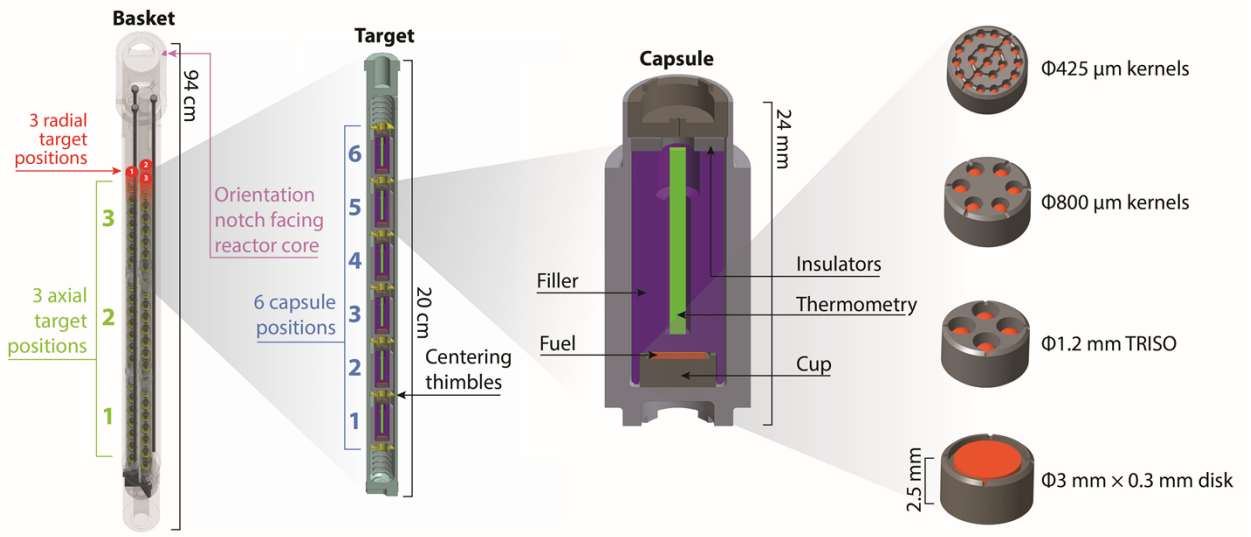

Figure 1. The irradiation design concept of the MiniFuel irradiation test vehicle [2].

The as-fabricated, as-run irradiation conditions experienced by the MiniFuel were simulated by the simulation methodology as described by Petrie et al. [2] and are briefly summarized here. Heat generation rates in the targets were calculated during a HFIR cycle using a coupled Monte Carlo radiation transport code, coupled with a weight window optimizer and a production depletion code. The heat generation rates were then transferred to an ANSYS model of the target to evaluate the temperature of the fuel specimens.

The MF01 target completed its third cycle on September 28, 2018 (HFIR cycle 482), after approximately 68 effective full power days of irradiation. The target was then inserted into HFIR cycle 483, but no burnup was accumulated, because this cycle was ended during start-up testing. The target was then discharged for PIE.

Table 1. Pre-irradiation properties and target irradiation conditions for the MiniFuel MF01 and MF02 targets.

Capsule ID and position by RAS* (MF01 / MF02)	Fuel form	Kernel theoretical density	Density (g/cm^3)	^{235}U enrichment (wt.%)	Burnup target	Target temperature (°C)
221 / 321	$UC_{0.20}N_{0.80}$ kernels	94.90%	13.598	0.22	1%FIMA/ 6%FIMA	500–600°C
222 / 322	$UC_{0.15}N_{0.85}$ kernels	90.60%	12.981	0.71		
223 / 323	$U_{0.89}Gd_{0.11}C_{0.11}N_{0.89}$ kernels	92.00%	13.178	0.71		
224 / 324	$U_{0.98}Gd_{0.02}C_{0.15}N_{0.85}$ kernels	93.60%	13.41	0.71		
225 / 325	$UC_{0.21}N_{0.79}$ kernels	90.90%	13.02	0.22		
226 / 326	$UC_{0.20}N_{0.80}$ TRISO particles	87.20%	12.49	0.22		

*(R= radial target position, A= axial target position, S= sub-assembly position)

3. POST-IRRADIATION EXAMINATION TECHNIQUES

After irradiation, the MF01 target was transferred from HFIR to the ORNL Irradiated Fuel Examination Laboratory (IFEL). The PIE executed to evaluate the initial MiniFuel irradiation performance included retrieving the capsules from the target capsule, measuring the fission gas released to the capsule, removing the fuel and thermometry from the capsule, evaluating the individual samples by gamma spectrometry, and evaluating select particles by x-ray computed tomography (XCT). This was followed by optical and electron microscopy. The burnup of one sample from each of the kernel-containing capsules was also evaluated by mass spectrometry to further benchmark the experiment.

3.1 Target Capsule Disassembly

After the targets were received at the hot-cell, the bottom endcap of the target capsule was cut with a slow speed saw [19], and the subassemblies from MF01 were removed. These cuts went as planned, and the capsules were easily removed from the target capsule.

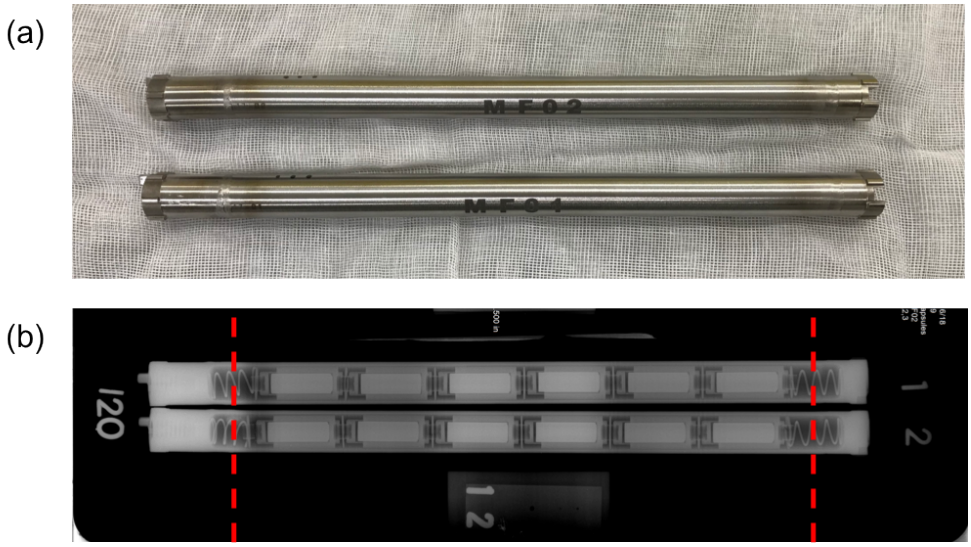

Figure 2. Pre-irradiation (a) photography and (b) x-ray image of the MF01 and MF02 targets; red dashed lines indicate PIE cuts [19].

3.2 Fission Gas Release Measurements

Fission gas release of all the MiniFuel samples was evaluated by measuring the fission gas present in the free gas volume of each capsule. The Kr-85 inventory was measured by passing the capsule fill gas through a liquid-nitrogen–cooled charcoal trap system. The captured Kr-85 was then counted on a high purity germanium (HPGe) detector system calibrated by a special form source that was designed to mimic a trap. The trap system was composed of two traps in series, so any breakthrough or leakage through the first trap would be noticed and captured. Both traps were counted after the puncture test, and the first trap was recounted hours or days after the first count to monitor for any short-term leaks that may have occurred. No significant leakage was noted in any of the traps used. Between tests, the traps were heated up to 200–250°C for 90 minutes under vacuum to evacuate the Kr-85 from previous tests. Then the traps were recounted to make sure they were empty prior to beginning the next test.

The schematic of the puncture system is shown in Figure 3. The system is first pumped down to check for leaks, the sample bottle (known reference volume) is used to compute the tare volume of the system, the system is again pumped down, and the MiniFuel capsule is punctured. The released gas pressure is measured as a function of time, as shown in Figure 4. Finally, gas flow is established through the system, which pushes the released gas through the cooled trap system. After approximately one hour, the traps are removed and allowed to warm up. They are then gamma counted the first time, and then they are recounted to investigate for reproducibility and/or leaks. A measurement was also made of the capsule free gas volume, but the volume was so small that the measurement uncertainty is too large for analysis.

The activities of Kr-85 measured by the gas puncture tests are shown in Table 2. In general, the gas release was small in all capsules. There was considerable uncertainty from counting statistics for some capsules where the detectable amount of Kr-85 was < 1 μCi. No detectable Kr-85 was present in Capsule 226, which was as expected since TRISO-coated particles had been loaded into that capsule. The fission gas release for the measured amount of Kr-85 is also given in Table 2. The fission gas release was determined by dividing the measured Kr-85 by the activity predicted from the as-run simulations.

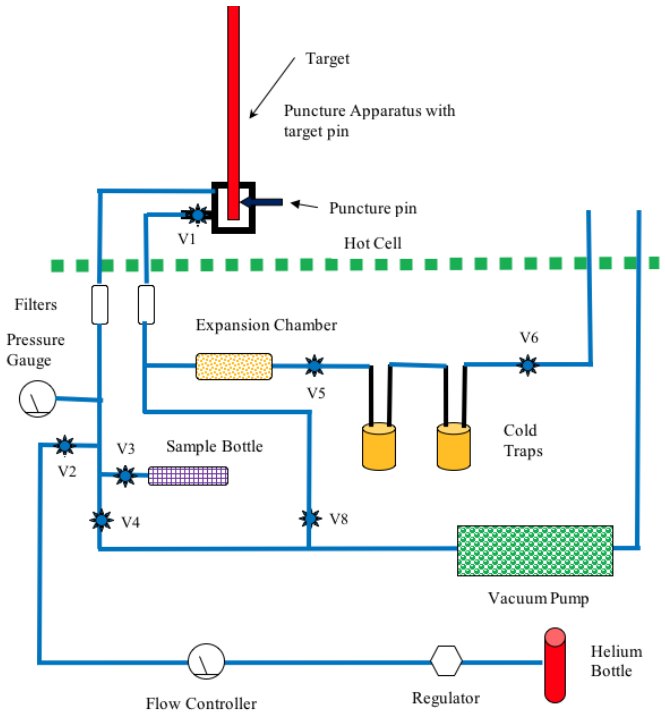

Figure 3. Schematic of the puncture system.

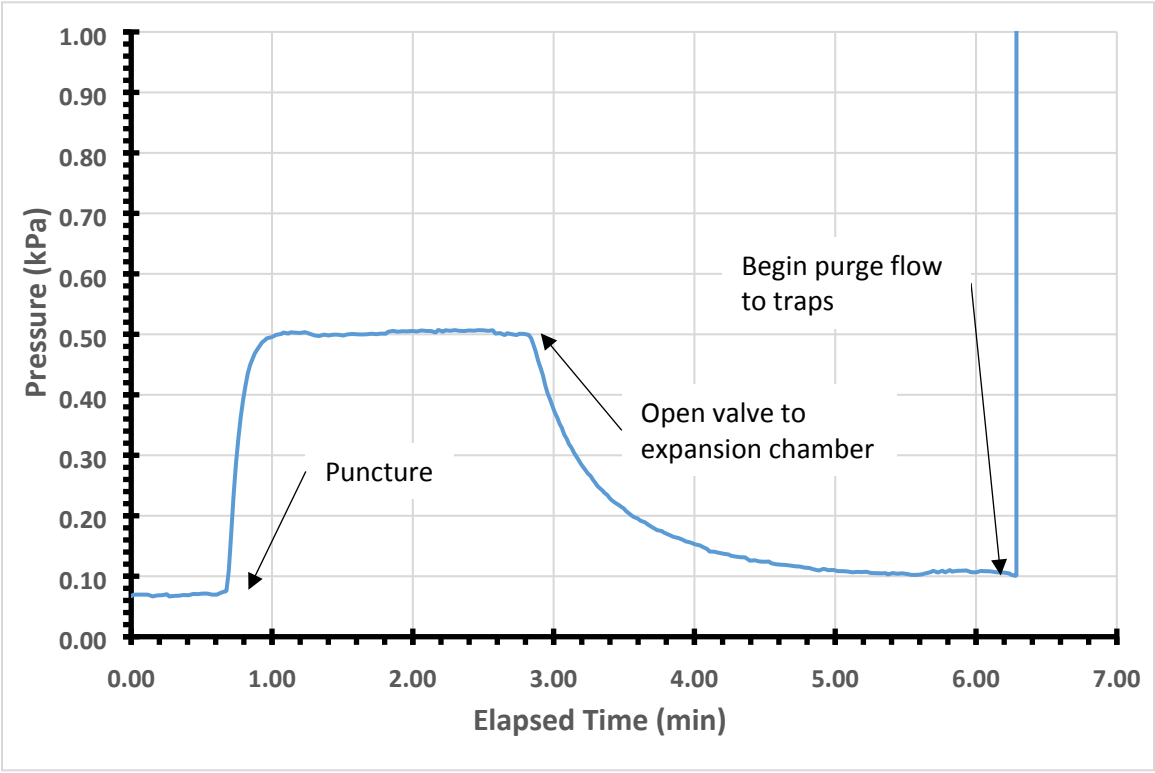

Figure 4. Puncture of MiniFuel capsule 221. The volume of the capsule is quite small, so only a small pressure can be observed.

Table 2. Results of gas puncture tests.

Capsule	Kr-85 activity (µCi)	Fission gas release
221	0.045 ± 0.006	0.16% ± 0.02%
222	1.015 ± 0.010	2.09% ± 0.02%
223	1.080 ± 0.019	3.49% ± 0.06%
224	0.014 ± 0.004	0.03% ± 0.01%
225	0.022 ± 0.005	0.08% ± 0.02%
226	<0.008	N/A

3.3 Capsule Disassembly and Sample Recovery

After puncturing, the top weld of the capsules was sectioned off using a low-speed saw and a positioning fixture to maintain sample orientation and retain the SiC thermometry. The opened capsules were capped to retain their geometry and transferred from the main hot-cell to an auxiliary hot-cell where operators have superior handling, viewing, and control of small samples. This cell is known as the *irradiated microsphere gamma analysis* (IMGA) cell. The IMGA cell also is equipped with a stereomicroscope and vacuum needle system that allows operators to select and sort individual spherical particles or other small items like the SiC thermometry. Care was taken to recover the inner dish that contained particles while maintaining the identities of the particles from pre-irradiation. However, it was only possible to maintain particle identification on 3 of the 6 capsules (221, 225, and 226). The available stereomicroscope was used to provide visual examination of the MiniFuel specimens. Visual examinations showed that the chemistry variations in the UN kernels tested in this target did not have a catastrophic effect on the fuel behavior at this burnup level. An example of the kernels from Capsule 221 is shown in Figure 5a. The UN kernel TRISO coated particle fuel also survived irradiation intact, as shown in Figure 5b. An example of the recovered SiC thermometry is shown in Figure 6. All 34 particles were recovered from the capsules and placed in individual sample vials for subsequent PIE, starting with gamma counting.

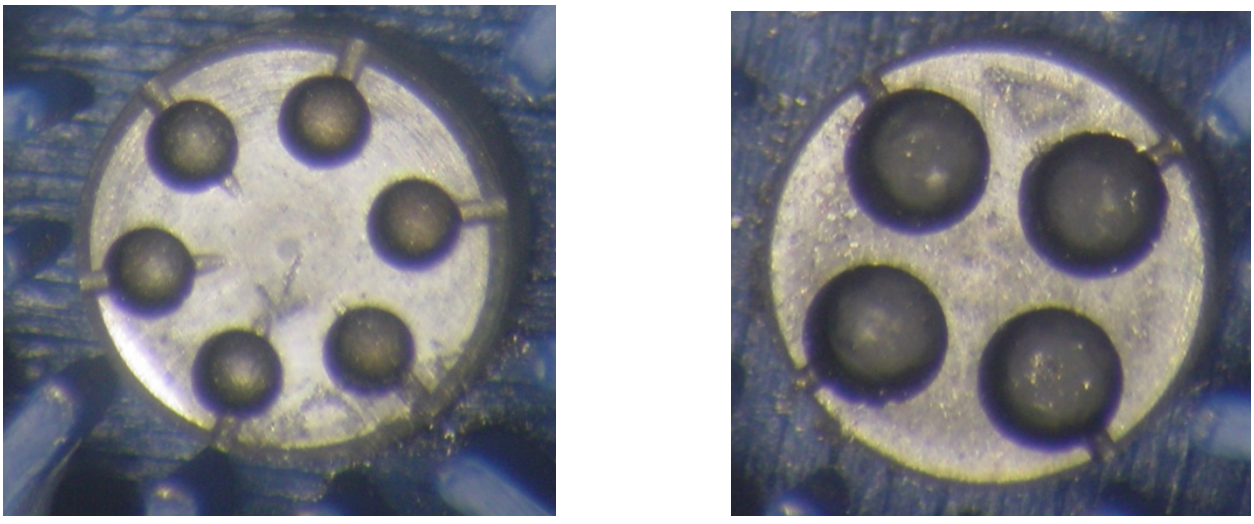

(a) (b)

Figure 5. (a) $UC_{0.20}N_{0.80}$ kernels from MiniFuel Target MF01, Capsule 221, (b) $UC_{0.20}N_{0.80}$ kernel TRISO particles from MiniFuel Target MF01, Capsule 226.

Figure 6. SiC thermometry recovered from MiniFuel Target MF01, Capsule 222.

3.4 Gamma Counting

The individual fuel particles from each capsule were gamma counted in the IMGA cell using a collimated HPGe detector integrated into that cell. Gamma spectrometry can be used in a variety of ways to characterize the fuel particles and target specific particles for enhanced study. In addition to the particles, any debris from disassembly and the Mo cups that held the particles were gamma counted to determine if there was any significant fission product release from the kernels. For the particles that did not have identities preserved in disassembly, the measured activity of their different radionuclides can be used to map different particles back to the pre-irradiation masses to provide a partial identification. The activity of Cs-137 and the ratio of the activity of Cs-134 to Cs-137 can be used to assess the burnup of the individual fuel particles [20]. This value can then be compared to neutronics simulations and provide some evaluation of the quality of the neutronics modeling. Some information about the major isotope that has fissioned during the test (U-235 vs Pu-239) can also be inferred from the gamma spectrometry. For example, Ru-106 has a much higher fission yield from Pu-239 fission than U-235 fission. This causes the Ru-106 to Cs-137 ratio to be higher in the depleted uranium kernels than in the natural uranium kernels.

All of the 34 particles have been counted. Select fission product activities are shown in Table 3. The activities have been decay corrected back to the end of the last HFIR cycle that was at full power (September 28, 2018). The gamma spectrometry results were also used to screen particles for mass spectrometry and optical microscopy to ensure that particles with representative content gamma–emitting isotopes were evaluated not particles that were outliers.

Table 3. Decay-corrected activity (µCi) of selected fission products from the MF01 MiniFuel particles.

Particle	*Zr-95*	*Ru-106*	*Cs-134*	*Cs-137*	*Ce-144*	*Eu-154*
221-01	5.73E+03	9.83E+02	2.63E+01	6.68E+01	1.50E+03	1.77E+00
221-02	6.01E+03	1.03E+03	2.79E+01	6.98E+01	1.56E+03	1.77E+00
221-03	6.05E+03	1.01E+03	2.80E+01	7.03E+01	1.59E+03	1.72E+00
221-04	4.72E+03	8.22E+02	2.15E+01	5.62E+01	1.25E+03	1.40E+00
221-05	5.32E+03	9.16E+02	2.43E+01	6.27E+01	1.41E+03	1.54E+00
221-06	4.98E+03	8.60E+02	2.31E+01	5.91E+01	1.31E+03	1.56E+00
222-01	8.33E+03	9.85E+02	4.31E+01	9.80E+01	2.35E+03	2.40E+00
222-02	6.46E+03	7.74E+02	3.37E+01	7.70E+01	1.81E+03	1.81E+00
222-03	8.26E+03	9.79E+02	4.27E+01	9.69E+01	2.33E+03	2.36E+00
222-04	8.57E+03	1.02E+03	4.46E+01	1.01E+02	2.42E+03	2.79E+00
222-05	7.87E+03	9.42E+02	4.08E+01	9.29E+01	2.22E+03	2.39E+00
222-06	6.49E+03	7.83E+02	3.45E+01	7.90E+01	1.82E+03	1.87E+00
223-01	3.82E+03	4.56E+02	1.94E+01	4.32E+01	1.05E+03	1.07E+00
223-02	5.36E+03	6.54E+02	2.63E+01	6.03E+01	1.46E+03	1.44E+00
223-03	5.62E+03	7.00E+02	2.85E+01	6.33E+01	1.55E+03	1.51E+00
223-04	5.32E+03	6.58E+02	2.63E+01	5.94E+01	1.48E+03	1.43E+00
223-05	4.65E+03	5.73E+02	2.27E+01	5.23E+01	1.29E+03	1.25E+00
223-06	3.26E+03	3.99E+02	1.69E+01	3.83E+01	8.94E+02	9.40E-01
224-01	8.03E+03	9.75E+02	4.23E+01	9.18E+01	2.24E+03	2.39E+00
224-02	8.01E+03	9.58E+02	4.13E+01	9.10E+01	2.25E+03	2.22E+00
224-03	7.72E+03	9.35E+02	4.04E+01	8.81E+01	2.18E+03	2.27E+00
224-04	8.09E+03	9.56E+02	4.14E+01	9.14E+01	2.25E+03	2.23E+00
224-05	8.14E+03	9.78E+02	4.24E+01	9.25E+01	2.26E+03	2.21E+00
224-06	8.50E+03	9.98E+02	4.35E+01	9.75E+01	2.37E+03	2.29E+00
225-01	5.62E+03	9.61E+02	2.60E+01	6.55E+01	1.47E+03	1.63E+00
225-02	5.05E+03	8.70E+02	2.28E+01	5.90E+01	1.33E+03	1.56E+00
225-03	5.75E+03	9.66E+02	2.68E+01	6.67E+01	1.51E+03	1.69E+00
225-04	6.27E+03	1.08E+03	2.88E+01	7.37E+01	1.63E+03	1.96E+00
225-05	5.31E+03	8.84E+02	2.45E+01	6.17E+01	1.40E+03	1.53E+00
225-06	5.12E+03	8.87E+02	2.37E+01	5.99E+01	1.34E+03	1.53E+00
226-01	6.07E+03	1.01E+03	2.77E+01	7.11E+01	1.59E+03	1.78E+00
226-02	5.65E+03	9.82E+02	2.58E+01	6.65E+01	1.47E+03	1.57E+00
226-03	5.54E+03	9.59E+02	2.57E+01	6.62E+01	1.45E+03	1.71E+00
226-04	5.05E+03	8.73E+02	2.27E+01	5.86E+01	1.31E+03	1.44E+00

3.5 SiC Thermometry

Each MiniFuel capsule contained a 13 × 1 × 1 mm parallelepiped SiC temperature monitor. These SiC monitors are evaluated by continuous dilatometry [21] to determine the average temperature of the monitors over the last 2 cycles of irradiation. The average irradiation temperature of the SiC for all the capsules was very similar. The average temperature evaluated by the dilatometry method was 403±5°C. The measured temperature of the SiC can be compared to finite element simulations of the MiniFuel capsules to determine the irradiation temperature of the fuel [2]. Based on these measurements and the simulation, the MF01 fuel was between 410 and 460°C over the last cycle of irradiation.

Table 4. Results of SiC thermometry evaluation.

Capsule	Measured temperature (°C)
221	403
222	403
223	406
224	406
225	402
226	394

3.6 X-ray Computed Tomography

X-ray computed tomography (XCT) has been used to evaluate a portion of the irradiated MF01 particles. It is possible with XCT to measure the volume of uncoated particles and to measure the kernel volume and layer integrity of coated particles. At this burnup, any irradiation-induced swelling of the material that may have changed the volume is too slight to allow for measurement of a volume change. At this writing, one UN TRISO particle has been evaluated by XCT, and no large radial defects in any of the coating layers were visible. Two other coated particles will be evaluated in future examinations in conjunction with heating tests.

3.7 Mass Spectrometry

The chemical composition of a sample of MiniFuel kernels was evaluated by mass spectrometry, and the resulting data are used to determine the burnup of the fuel in the sampled capsules and compare back to neutronics simulations. A particle from each of the 5 capsules with bare kernels was dissolved for mass spectrometry analysis. The 5 particles were dissolved in 8N heated nitric acid, and the dissolved samples were then evaluated on a series of mass spectrometers to determine the actinide and fission product content of the fuel.

3.8 Microscopy

Particles from each capsule were selected for optical microscopy. The selected particles were mounted in epoxy, ground, and polished. Optical microscopy was performed using a Leica Model DMI5000M inverted microscope. Images were collected with an integrated Leica DFC490 digital camera at several different magnifications. Examples from the 6 MiniFuel capsules are shown in Figure 7 through Figure 12. The same mounts that were prepared for optical microscopy were also examined by scanning electron microscopy (SEM).

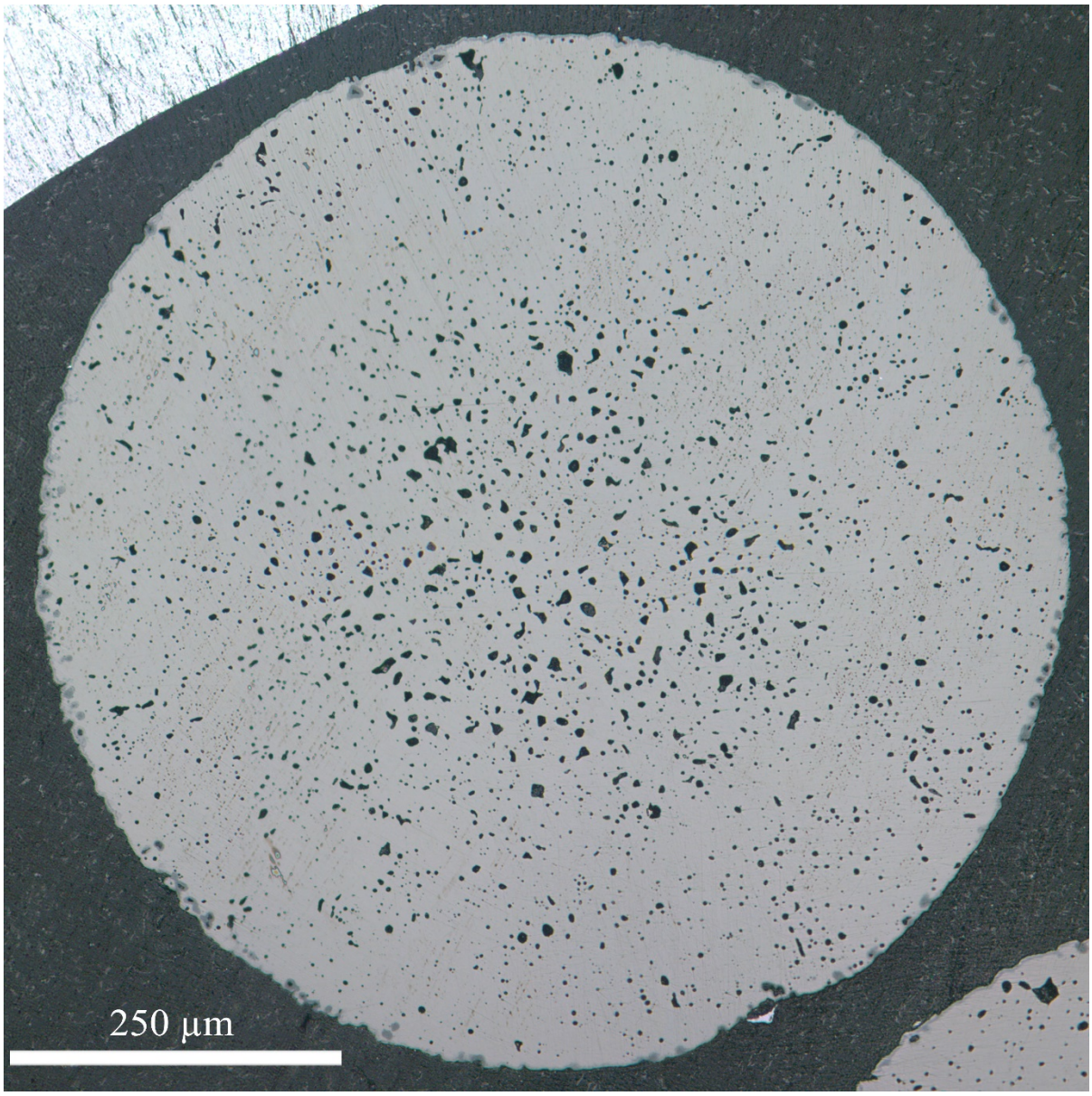

Figure 7. Optical microscopy of irradiated $UC_{0.20}N_{0.80}$ particle, MF01 221-02.

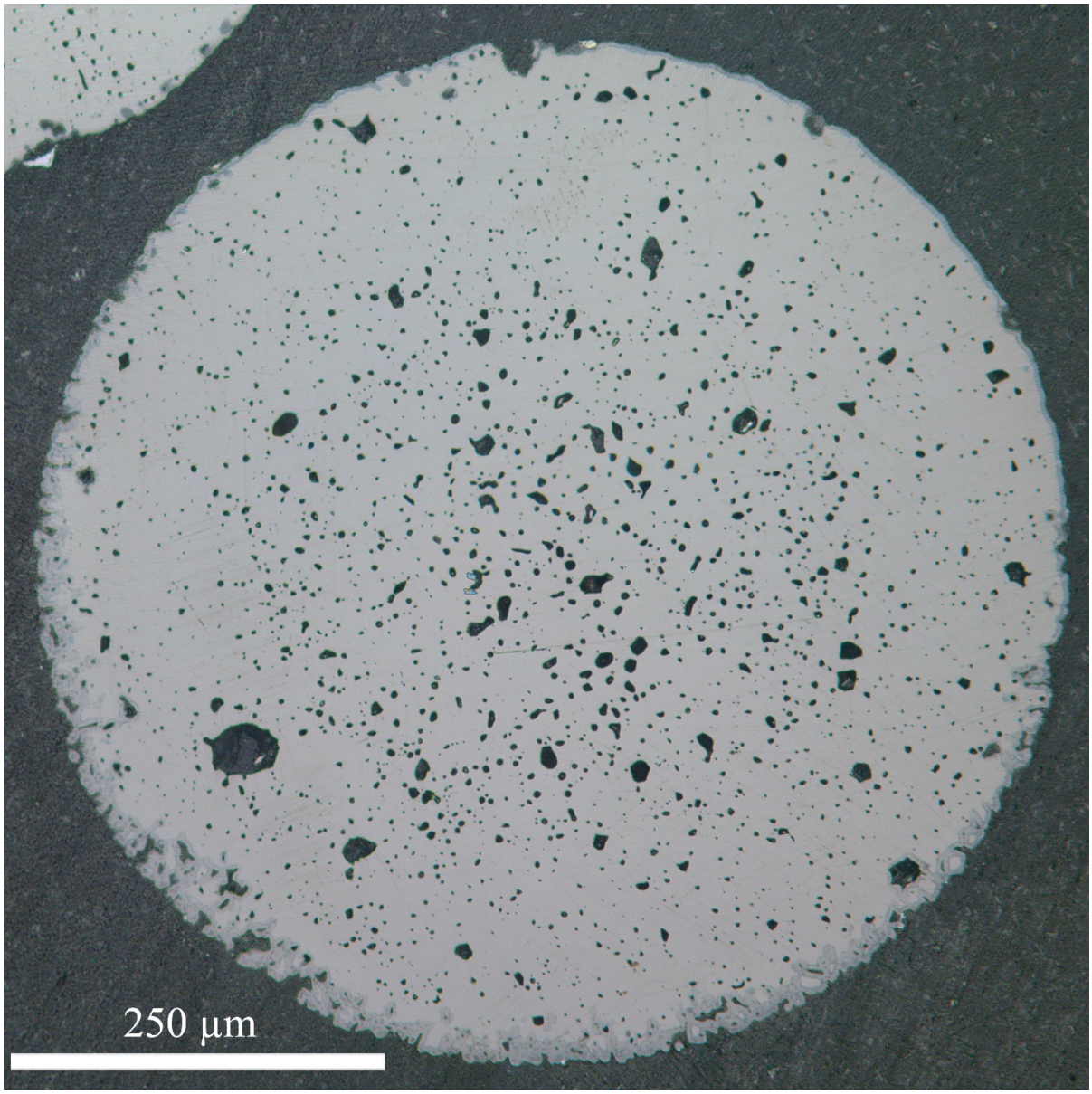

Figure 8. Optical microscopy of irradiated $UC_{0.15}N_{0.85}$ particle, MF01 222-02.

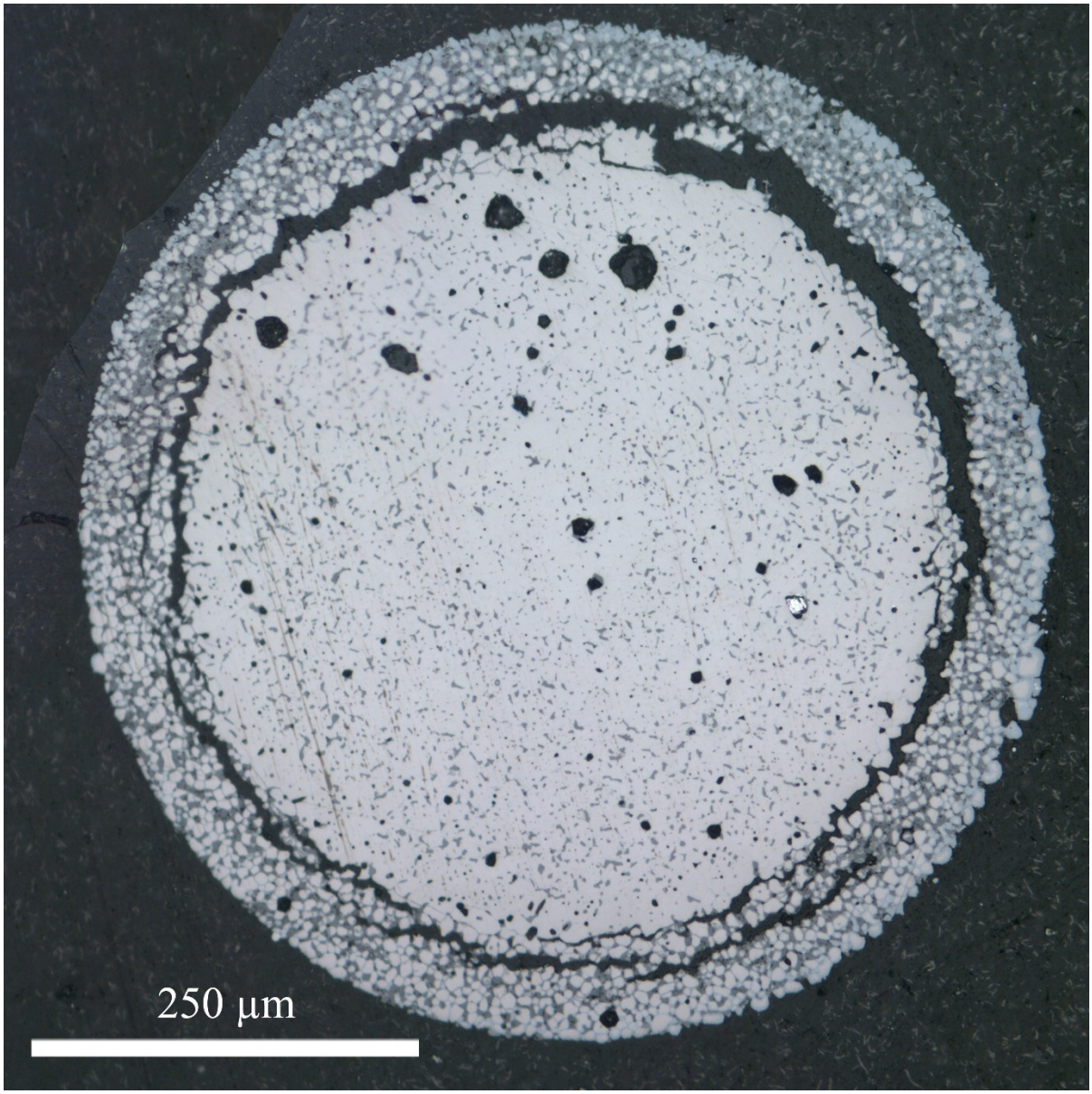

Figure 9. Optical microscopy of irradiated $U_{0.89}Gd_{0.11}C_{0.11}N_{0.89}$ particle, MF01 223-04.

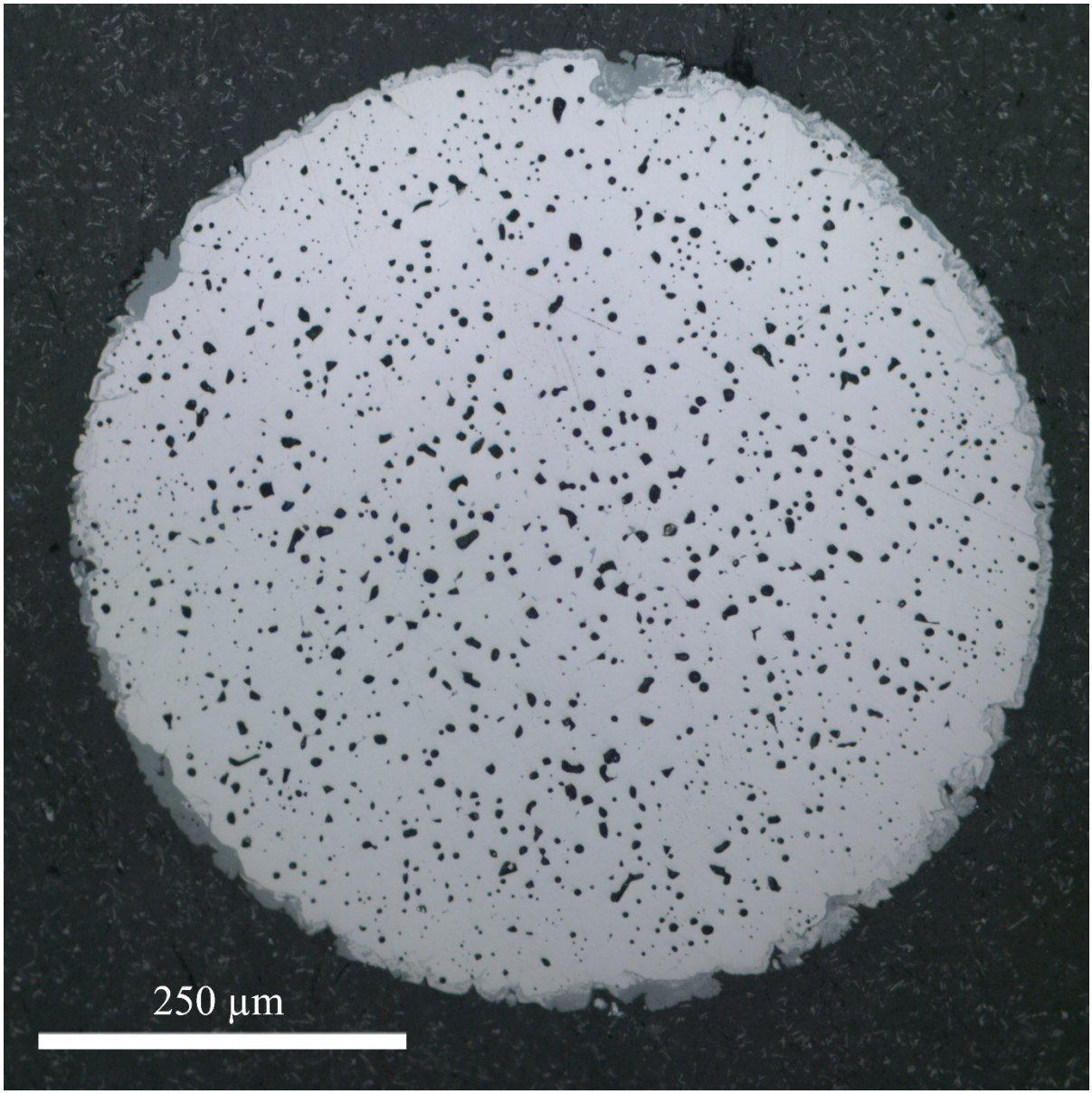

Figure 10. Optical microscopy of irradiated $U_{0.98}Gd_{0.02}C_{0.15}N_{0.85}$ particle, MF01 224-02.

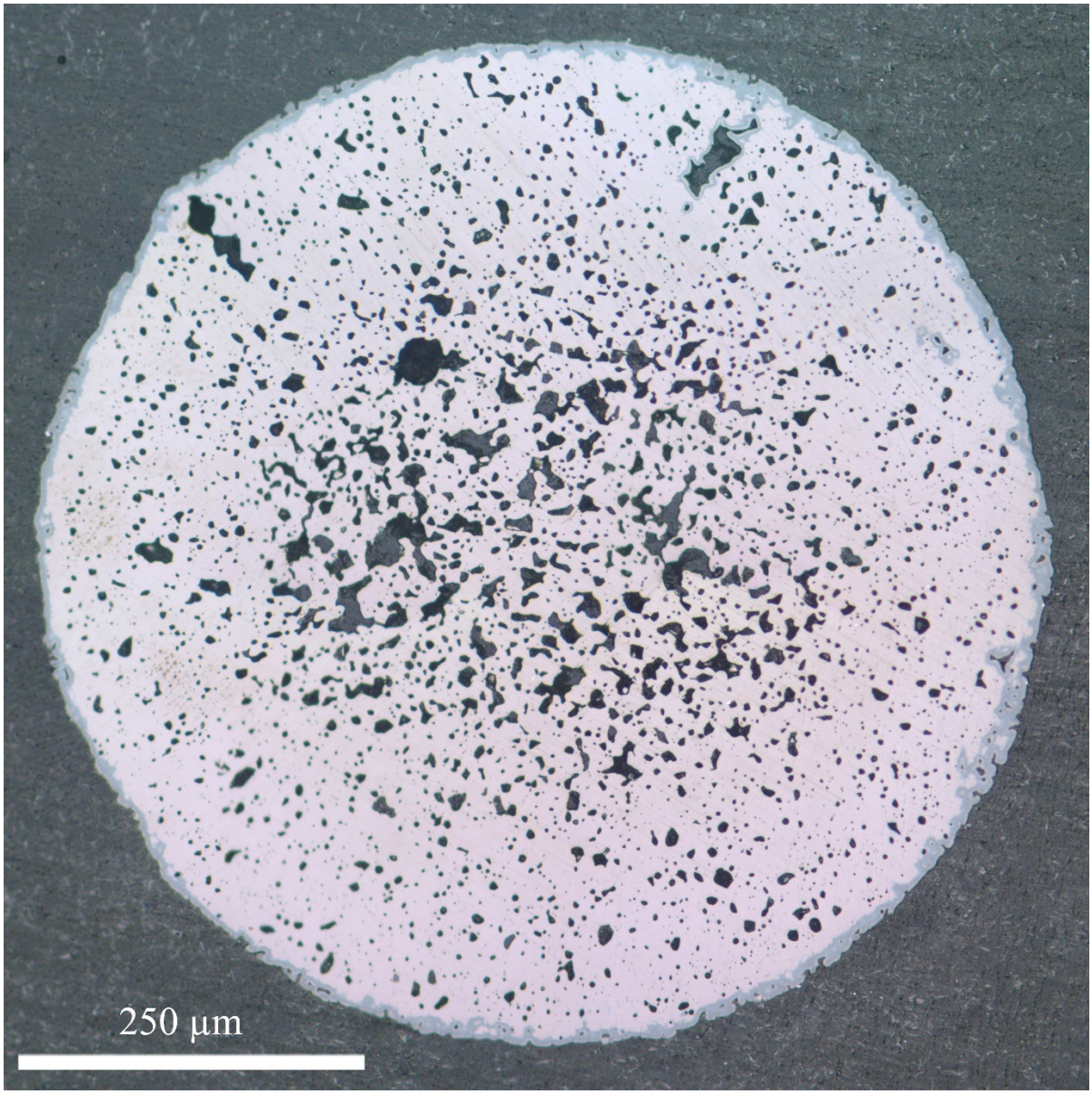

Figure 11. Optical microscopy of irradiated $UC_{0.21}N_{0.79}$ particle, MF01 225-06.

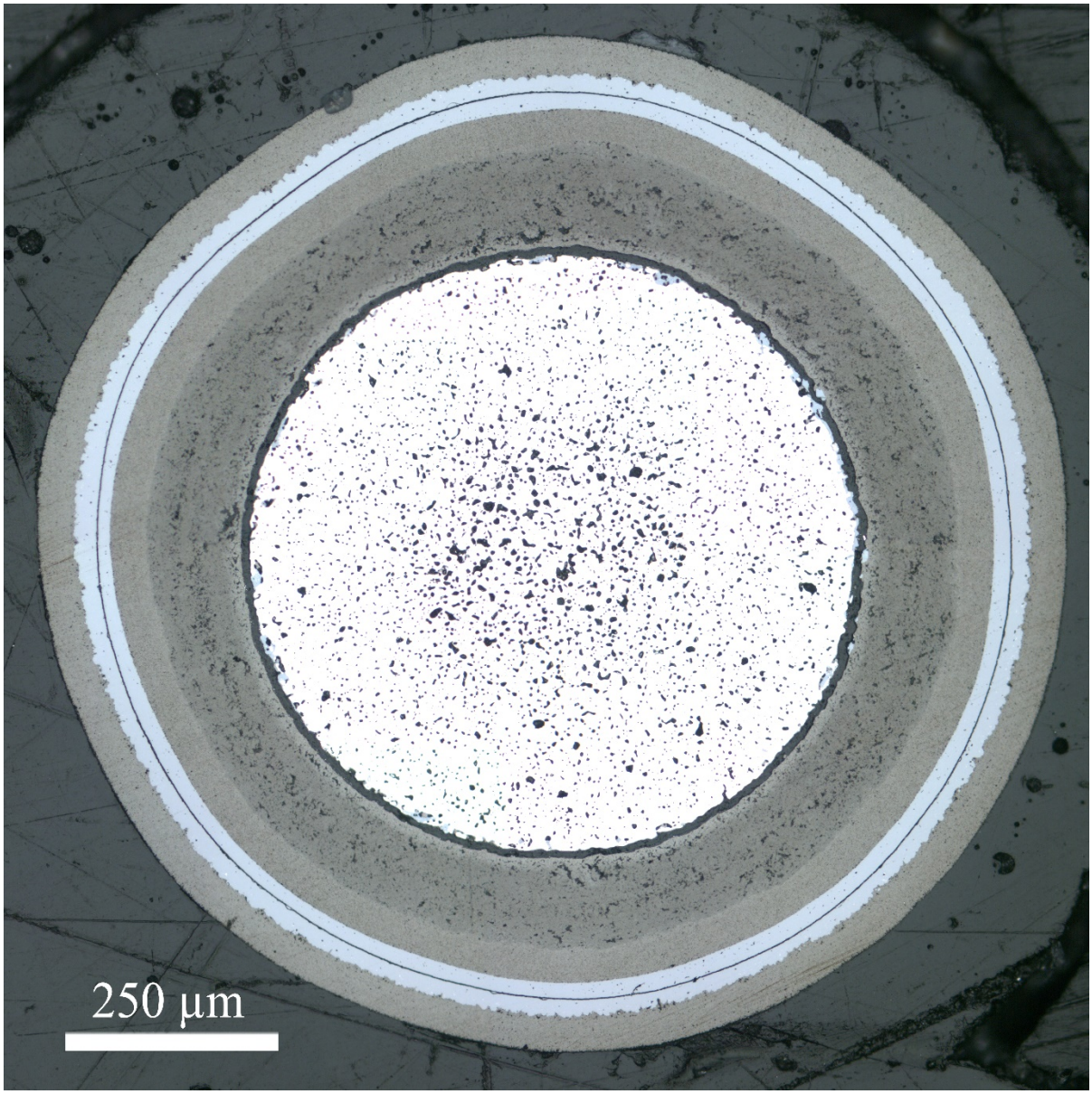

Figure 12. Optical microscopy of irradiated $UC_{0.20}N_{0.80}$ TRISO coated particle, MF01 226-04.

4. DISCUSSION

Postirradiation examination of MiniFuel has been successful, especially for the first PIE of a new irradiation vehicle. A few lessons learned have been noted related to capsule labeling and the need for a more robust method for final capsule disassembly to increase the reliability of maintaining particle identity. This improvement is necessary for pre-irradiation and postirradiation characterization comparisons of factors such as the volume and mass of the individual samples, which are critical for the evaluation of high-precision swelling.

4.1 Observed Irradiation Conditions Compared to Simulation

For new irradiation vehicles, it is especially important to verify that the methods used to predict and simulate the irradiation conditions are producing results consistent with experimental observations. The neutronics simulations appear to be adequately capturing the fission and transmutation process that drives burnup accumulation in the MiniFuel capsules. Feedback from the isotopic results of the MF01 target will be used to improve the simulations used in the design and continued irradiation of the many MiniFuel capsules that are currently being built or are already in the reactor.

Table **5** contains the burnup predicted by the as-run simulations, as well as measured burnup evaluated by several different methods. The average capsule burnup by Cs-137 content is determined by a modified "Fission Product Monitor – Residual Heavy Atom" technique [20,22] where the number density of actinides was assumed to not have changed during the short irradiation. The average capsule Cs-134/Cs-137 ratio burnup is determined using the same technique outlined in Harp et al. [20]. The mass spectrometry based burnup is also determined using the "fission product monitor – residual heavy atom" technique [20,22]. The following nuclides were used in the "Lanthanide Average" burnup determination: La-139, Ce-140, Pr-141, Ce-142, Nd-145, Nd-146, and Nd-148. A weighted average of the U-235 and Pu-239 thermal neutron fission product yields for each nuclide was used for each capsule based on the relative proportion of each measured nuclide. The Nd-148 burnup has the advantage of a roughly equivalent yield for U-235 fission and Pu-239 fission. All these different measures are in good agreement (~10% or less) with the simulations to the limit of experimental accuracy. The greatest disagreement occurs between simulations and the Cs-137 based burnup for Capsules 223, 224, and 225, but the mass spectrometry based measurements for these capsules agree well with simulation. This agreement demonstrates that the current simulation methodology is capturing the neutronic conditions in the irradiation vehicle at this burnup. The final Pu isotopics are also worth investigating. The production and fission of Pu is particularly important for this experiment because the constant temperature and accelerated fission rate desired in this irradiation depend on U-238 conversion to Pu-239. As seen in

Table **6**, the absolute Pu-239 content per particle predicted by simulations does not differ too much from the measurements at this burnup. However, the simulations underpredict the ratio of Pu-239 to U-238, and they underpredict the ratio of Pu-239 to Pu-240. For Pu-239/U-238, the simulations may be underpredicting the conversion of U-238 to Pu-239, or overpredicting the destruction of Pu-239 by fission or neutron capture. The ratio of Pu-239/Pu-240 in the simulation is lower than in the experimental data, which points to overprediction of Pu-239 destruction by fission. This discrepancy has not overly impacted burnup at current levels, but this difference will be monitored to ensure that future MiniFuel experiments are discharged at the appropriate cycle to meet their burnup targets.

Table 5. Predicted and measured burnup of fuel in MiniFuel capsules evaluated by different methods

		Gamma Spectrometry		Mass Spectrometry	
Capsule	**Simulation (MWd/kgU)**	**Cs-137 activity (MWd/kgU)**	**Cs-134/Cs-137 ratio (MWd/kgU)**	**Lanthanide average (MWd/kgU)**	**Nd-148 (MWd/kgU)**
221	6.0	5.5	5.7	5.2	5.9
222	9.1	9.3	8.2	8.2	9.1
223	9.2	6.8	8.7	8.6	9.5
224	9.2	7.2	8.4	8.9	10.0
225	6.2	4.6	5.8	5.5	6.0
226	6.5	5.9	6.1		

Table 6. Relative Pu isotopics from mass spectrometry compared to simulations

	Pu-239 mass per particle (μg)		**Pu-239/U-238**		**Pu-239/Pu-240**	
Capsule	**Simulation**	**Mass spectrometry**	**Simulation**	**Mass spectrometry**	**Simulation**	**Mass spectrometry**
221	14.0	14.3	3.7E-03	4.2E-03	2.9	3.3
222	12.7	14.1	3.8E-03	4.2E-03	2.9	3.3
223	10.7	9.3	4.0E-03	4.6E-03	2.9	3.3
224	16.7	15.1	3.8E-03	4.5E-03	2.8	3.3
225	17.2	13.5	3.8E-03	4.3E-03	2.8	3.4

The irradiation temperatures determined via dilatometric analysis of the passive SiC temperature monitors (TMs) can also be compared to the thermal design calculations. Following the methodology established previously [14], three-dimensional ANSYS finite element simulations were performed using nuclear heating rates determined from MCNP and ORIGEN. Table 7 compares calculated vs. measured temperatures of the TMs in each capsule. Table 7 also includes fuel temperatures determined via calculation and after compensating for the observed differences in calculated vs. measured TM temperatures. The calculated temperatures were taken at the end of the irradiation.

The calculated TM temperatures were approximately 50°C higher than the measured values. Most of the temperature variation (~350°C) within the experiment occurs through the ~0.3 mm gas gaps between the capsules and the inner surface of the target. The only other significant temperature variation (~50°C) occurs within the gap between the capsules and the filler. The average temperatures of the fillers, cups, and TMs are equal to within <5°C. Because the calculated burnup generally agrees with the post-irradiation measurements, there is good confidence that the fuel heating rates were accurately calculated. This also implies that the calculated difference in temperature between the fuel and the TMs is correct. The discrepancies between the calculated vs. measured TM temperatures are most likely related to the calculation of heat transfer through the filler/capsule and/or capsule/target gas gaps. The critical inputs to the gap heat transfer calculations are the diameters of the components and the gamma heating rates in the structural materials. The diameters of the capsules used in the model were identical to the as-built dimensions. The modeled target inner diameter was 0.01 mm larger than the as-built value, but this discrepancy would result in the capsule temperatures being at most 6°C cooler than the as-calculated

values. The as-built gaps between the filler and the capsule were 0.02 to 0.035 mm larger than the modeled values, which would result in the temperature difference through the filler/capsule gap being 7-12°C higher than predicted by the model. Therefore, the most likely explanation for calculated TM temperatures being 50°C higher than the measured values is that the gamma heating rates were approximately 13% lower than the calculated values. The nuclear heating calculations are quite complex, requiring both MCNP and ORIGEN calculations to simulate radiation transport from the core center to the reflector positions and to calculate reaction rates in each cell. Furthermore, the calculations determine more than just prompt neutron and gamma heating. They also consider local decay heat, as well as gamma heating originating from fission products that accumulate in the HFIR fuel and from component activation. Considering the complexity of these calculations, it is certainly possible that the calculated heating rates could have an error in the range of 13%.

Table 7. Comparison of measured vs. calculated average component temperatures.

Capsule	Measured TM temperature (°C)	Calculated TM temperature (°C)	Calculated fuel temperature (°C)	Compensated fuel temperature (°C)
221	403	454	502	451
222	403	453	512	462
223	406	448	513	471
224	406	455	514	465
225	402	455	499	446
226	394	453	504	445

4.2 Fission Gas Release

The irradiation conditions in this test are distinctly different than historic nitride fuel irradiations that have measured fission gas release [10,23]. The observed fission gas release was less than expected for some capsules. At the irradiation temperatures in this experiment, only athermal fission gas release from recoil is expected, which does agree with historic expectations [23]. However, the observed release is also below what is expected for recoil.

A plot of the fission gas recoil release versus theory [24] for 3 cases, no wall absorption of recoils, half wall coverage with capture of recoils, and the kernel treated as dust with all recoils released is shown in Figure 13. The measured releases do not fit the expected pattern. The only way this mismatch can be explained is (1) if 3 of the 5 puncture tests had virtually 100% trap leakage (note that Capsule 226 is not included because it is composed of TRISO particles which are not expected to release fission gases), (2) if the temperature of the capsules was significantly different from that anticipated, or (3) if the fuel holders absorbed much of the recoils (Kr-85 gas). Somewhat higher than expected gas release could be explained by cracks or fissures in the kernel, but much lower release is more difficult to explain unless the kernels have a non-fissile surface layer of some kind.

After thoroughly inspecting the traps and procedures used in the fission gas release measurements, it was determined that no systematic loss of Kr-85 due to faulty equipment was impacting the reported fission gas release values. Thus, the results of the puncture testing are ambiguous. It is clear that the capsules remained sealed during irradiation and that at least some of the kernels released 2–3% of their Kr-85. Further PIE performed to date has not provided additional information on capsule irregularities that may have trapped fission gas during measurement. The next section indicates that an oxygen rich outer layer is present on the bare kernels, and this may have had some effect. However, it would have been necessary for the layer would to be mostly non-fissile material to reduce the recoils to such low

levels. Fission gas release may simply be highly variable for nitride fuel irradiated at low burnup and low temperatures.

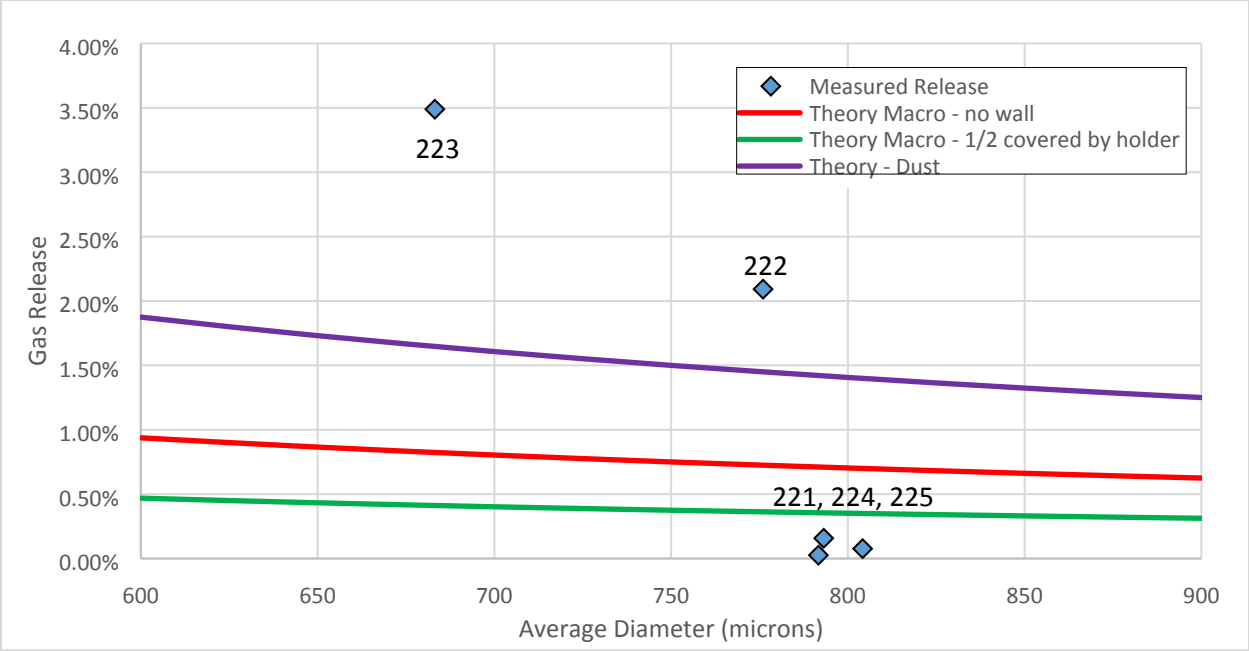

Figure 13. Kr-85 gas release versus recoil theory. The average diameters near 800 microns do not conform to the theory.

4.3 Microstructure Examination

With optical microscopy, it is often possible to observe microstructural changes in the fuel from irradiation that can lead to macroscopic changes in fuel behavior. Swelling in particular should begin to increase porosity or impact porosity in the fuel and could possibly change the shape of the pores. In addition to optical microscopy, SEM / energy-dispersive x-ray spectroscopy (EDS) was used to identify the approximate composition of secondary phases observed in the optical microscopy. For this low irradiation, few observations can be made concerning microstructural changes in the fuel. The porosity and the morphology of the kernel pores do not differ in a noticeable way from the as-fabricated microstructure. It was possible to use backscatter electron (BSE) imaging of the samples to observe secondary phases and the grain structure of the irradiated kernels. This is shown in Figure 14 for a $U_{0.98}Gd_{0.02}C_{0.15}N_{0.85}$ kernel (MF01-224-02). From these images, the grain size was measured to be 31±6µm, which is not significantly different from the as-fabricated grain size.

There are secondary phases present on the periphery of the bare kernels in Figure 7 through Figure 11. These peripheral secondary phases in the optical microscopy were confirmed to be oxygen rich phases in the SEM. The oxygen rich phases observed on the periphery of the kernels are an artifact from fabrication where kernels were removed from the conversion furnace before fully cooling. The oxygen rich phases are illustrated in Figure 15 using optical microscopy, BSE imaging, and EDS mapping of oxygen. In this area, there are oxygen-rich areas on the boundary between the kernel and the epoxy, and they are also located in a pore that was open to the free surface of the kernel. Closed porosity in the kernels do not exhibit the oxygen rich phase on their perimeters. No fission product rich phases were observed. At this burnup, it is likely that solid fission products are miscible in the fuel matrix or not yet produced in sufficient quantity to allow for observation with SEM / EDS techniques.

Analysis by EDS of the Gd bearing kernels showed that there was some Gd fully dissolved into the UN matrix. However, there are also secondary phases present in the Gd bearing kernels, as well, which were confirmed to be Gd-bearing by SEM/EDS analysis. These phases were quite small and well

dispersed in both compositions, as shown by Figure 16. In the $U_{0.89}Gd_{0.11}C_{0.11}N_{0.89}$ kernels, the extra Gd led to some Gd phases that were on the periphery of the kernel, as well. This same behavior was observed in the as-fabricated kernels and is likely a result of nonoptimized internal gelation and conversion parameters for this composition. The external phases are a mixture of Gd and Gd-O. These phases are shown in BSE in Figure 17 and by EDS mapping in Figure 18. The mixed EDS map in Figure 18 shows the major UN phase in purple, the Gd secondary phases in green, an oxidized U phase in orange, and an oxidized Gd phase in yellow. There was also a sulfur signal consistently observed in the Gd phases. EDS analysis showed approximately 0.6 atoms of sulfur per atom of Gd in these precipitates. This sulfur is likely carried over from fabrication, where Tamol SN, a synthetic naphthalene sulfonate dispersant, is used [18]. Sulfur was only observed in Gd phases internal to the kernel and was not observed in Gd phases on the periphery of the kernel. Chemical analysis of the Gd kernels also confirmed the presence of Gd in these kernels. The Gd isotopics are enriched in Gd-156 and Gd-158 and are depleted in Gd-155 and Gd-157 compared to natural Gd isotopics, as would be expected from irradiation in a neutron field. It is notable that Gd is not transmuting to a different element. Any modifications in chemical/atomic properties of the fuel resulting from Gd additions was not impacted by this level of neutron irradiation.

Figure 19 shows a BSE image of the interface between the UN kernel and the buffer layer in one of the irradiated UN TRISO particles (MF01 226-02). There was some interaction between the kernel and buffer, where a bright layer decorates the buffer edge in Figure 19. This interaction was primarily caused by fission fragment recoil into the buffer. This is often observed in uranium oxide / uranium carbide kernel TRISO particles [25–29]. A slight gap (~10 µm) opened between the kernel and the buffer, which is also typical and may simply be due to thermal expansion mismatch. As with the rest of the kernels, no fission products phases were observed in the kernel, and no fission product precipitates were observed at the inner pyrolytic carbon layer – SiC layer interface, as shown in Figure 20. A circumferential crack in the SiC layer formed during sample preparation, which is also evident in Figure 12. This crack is believed to be due to sample preparation not due to irradiation induced stresses. However, a similar crack did form during the preparation of both UN TRISO particles that were prepared. No evidence of a crack of this sort was observed in the XCT of MF01 226-04, further supporting that this crack was induced during sample preparation.

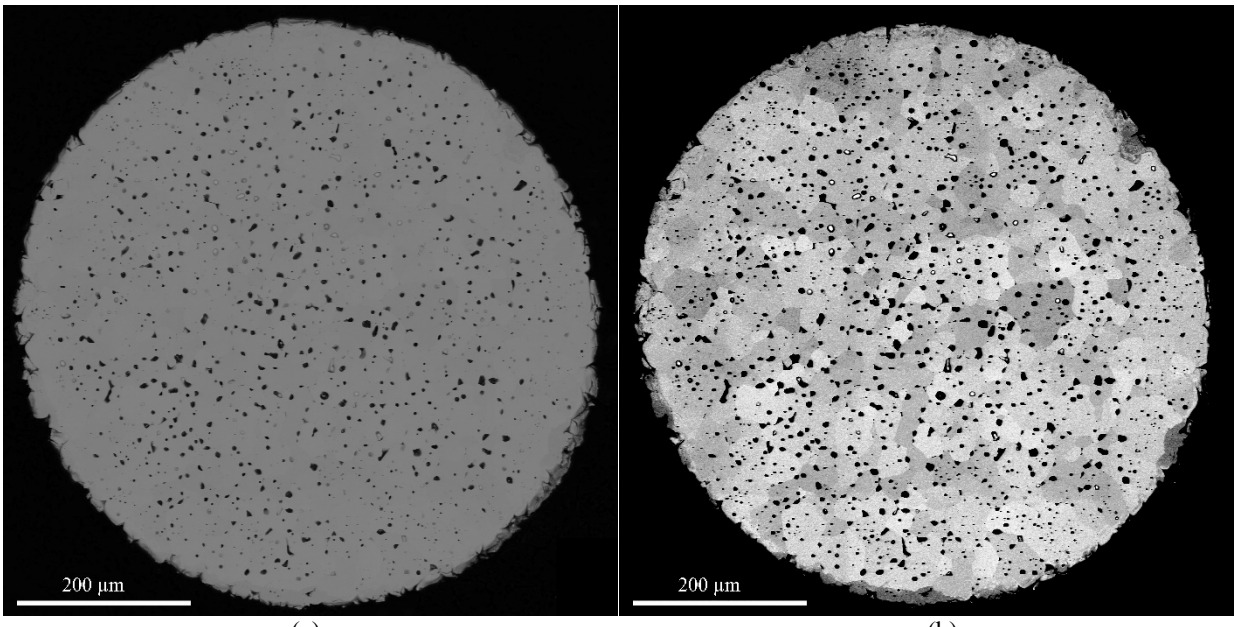

(a) (b)

Figure 14. (a) BSE image of a $U_{0.98}Gd_{0.02}C_{0.15}N_{0.85}$ kernel (MF01-224-02) at low contrast to reveal secondary phases, (b) and high contrast to reveal grain structure.

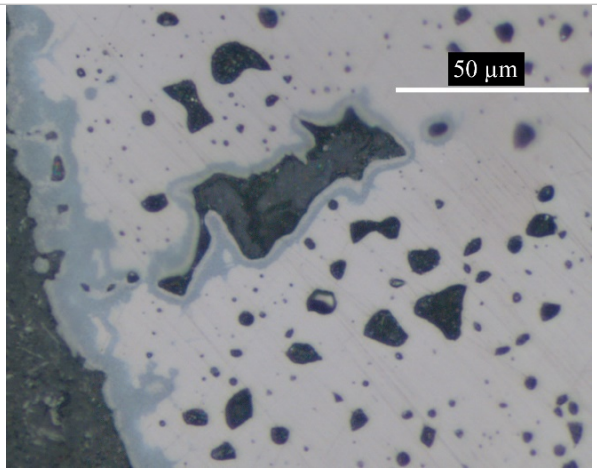

(a)

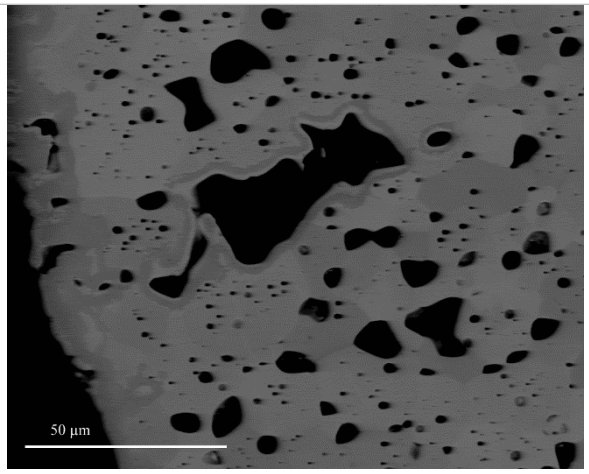

(b)

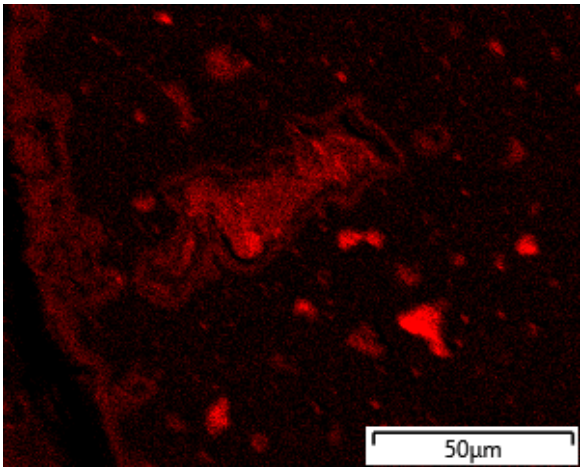

(c)

Figure 15. Secondary oxygen rich phases on the periphery of a $UC_{0.11}N_{0.89}$ kernel (MF01-225-06) imaged by optical microscopy (a), BSE imaging (b), and oxygen EDS mapping of the same area (c).

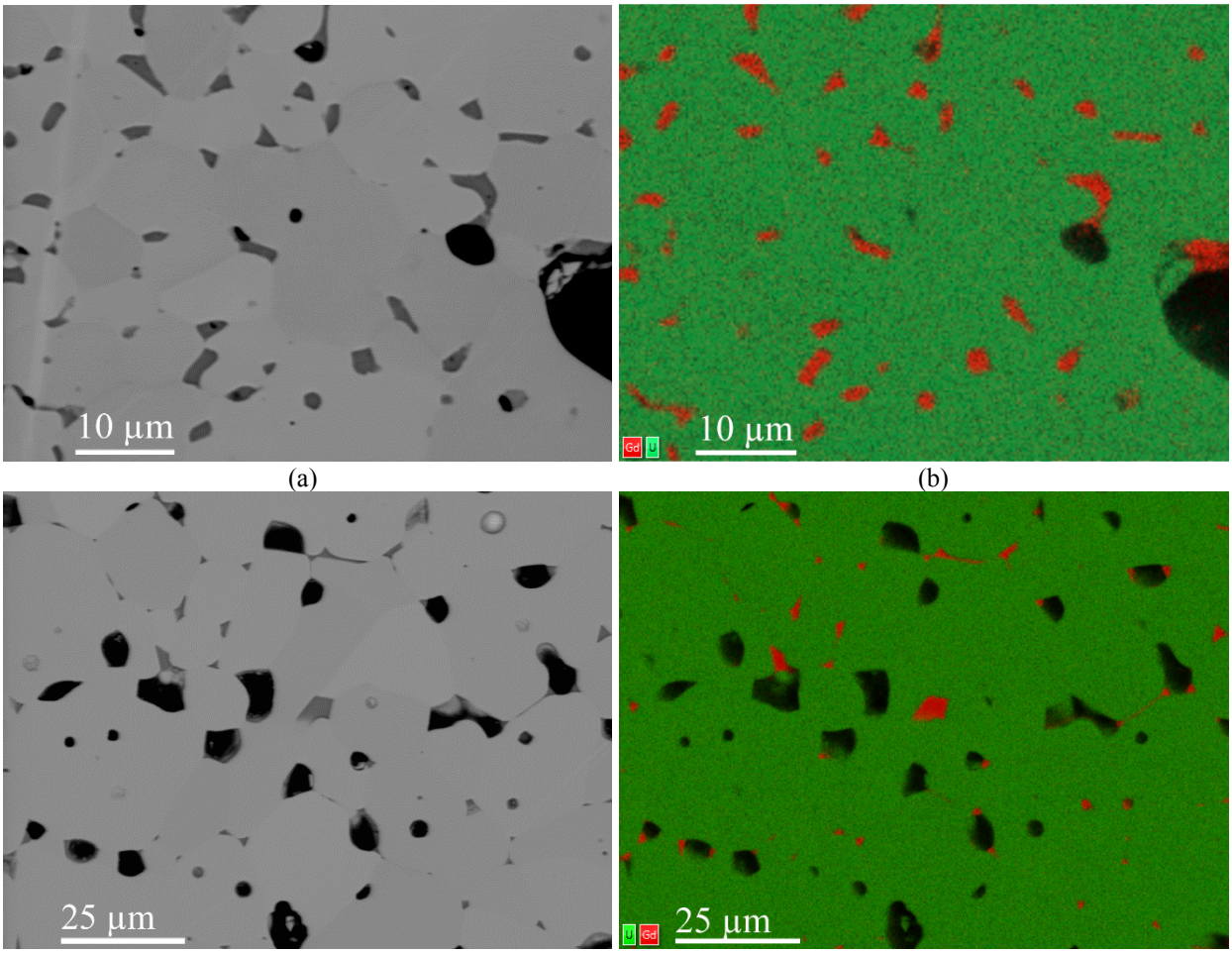

(a) (b)

(c) (d)

Figure 16. (a) BSE image of the general microstructure of a $U_{0.89}Gd_{0.11}C_{0.11}N_{0.89}$ kernel (MF01-223-04) showing Gd bearing secondary phases in dark gray, (b) an EDS map of the same area showing U content in green, and Gd content in red. (c) BSE image of the general microstructure of a $U_{0.98}Gd_{0.02}C_{0.15}N_{0.85}$ kernel (MF01-224-02) showing Gd bearing secondary phases in dark gray, (d) an EDS map of the same are as (c) showing U content in green, and Ge content in red.

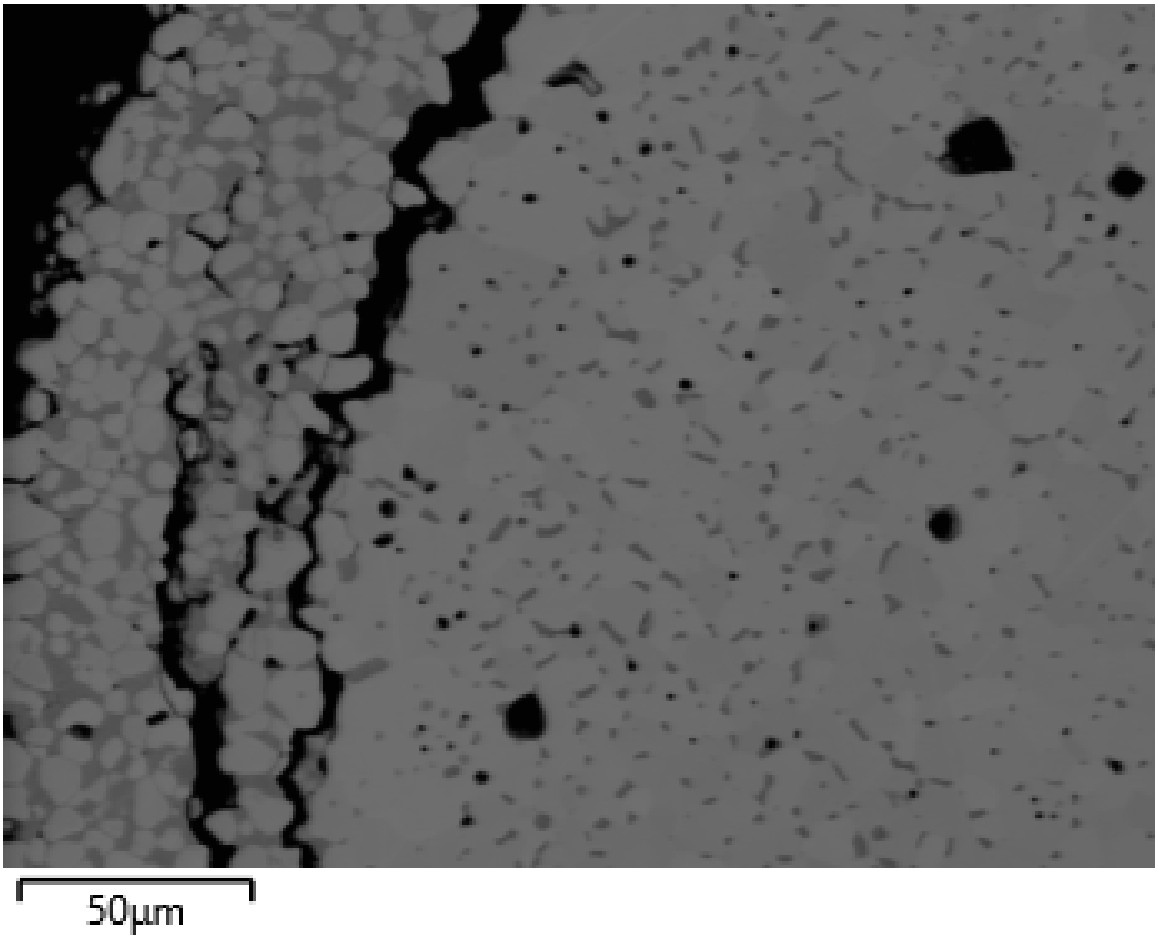

Figure 17. BSE image of the edge of an irradiated $U_{0.89}Gd_{0.11}C_{0.11}N_{0.89}$ particle, MF01 223-04, showing the oxidized Gd and U on the edge and Gd secondary phases in the interior.

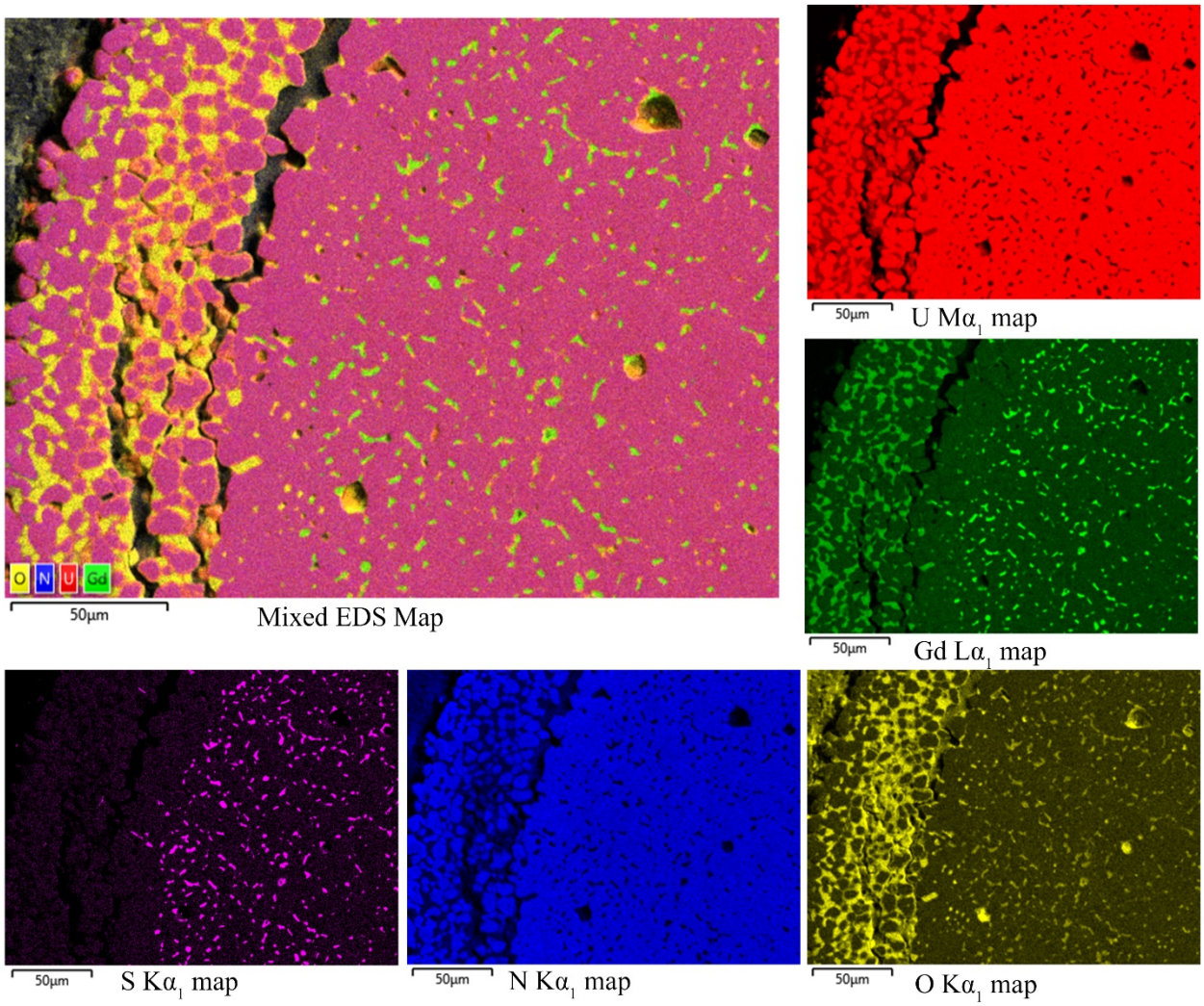

Figure 18. EDS mapping of the area shown in Figure 17, highlighting the different observed phases, including UN (purple), oxidized U (orange), Gd secondary phases (green), and oxidized Gd phases (yellow). The individual EDS maps of these elements are also shown. In addition, an individual EDS map for S is presented which demonstrates that S is limited to the internal Gd phases.

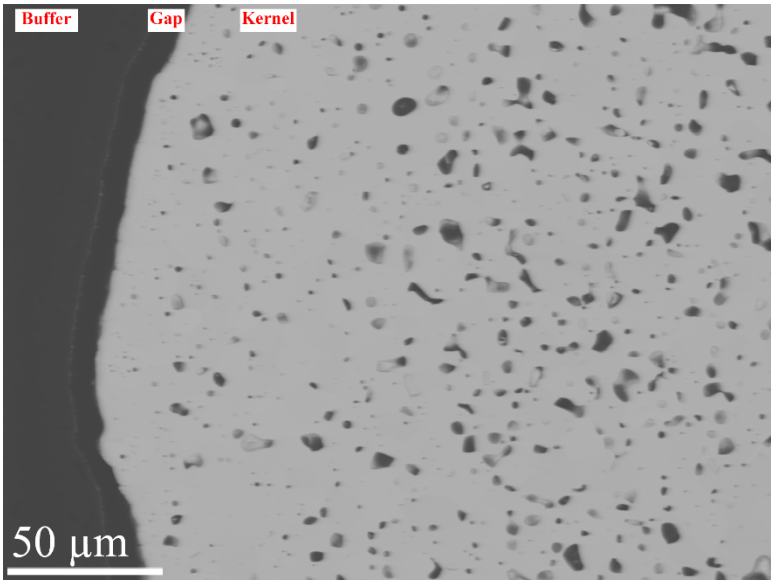

Figure 19. BSE image of the kernel buffer interface in an irradiated UN TRISO particle (MF01 226-02).

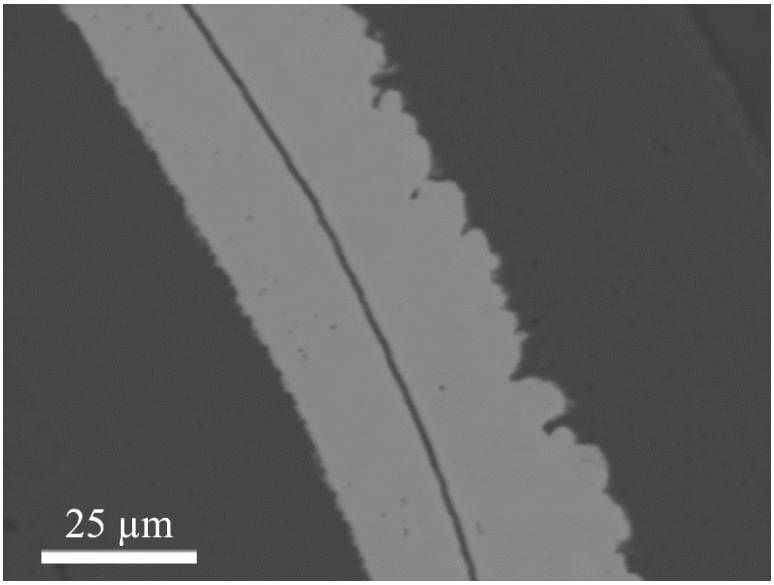

Figure 20. BSE image of the SiC layer and its interface with the inner and outer pyrolytic carbon layers.

5. SUMMARY

Postirradiation examination will continue on the first MiniFuel target discharged from HFIR. Heating tests on the remaining UN TRISO particles are planned to evaluate their behavior in postulated accident conditions. Transmission electron microscopy is also planned for the irradiated UN kernels to further confirm the crystal structure of the phases observed in SEM, investigate swelling, and scrutinize the kernel material for fission products phases that are below the detection limit of the techniques discussed in this work. This PIE served as a shake-down test of the PIE techniques that will be applied to future MiniFuel experiments. The isotopic evaluation and temperature monitor results have provided valuable feedback to the simulation of MiniFuel targets currently being designed and fabricated for insertion into HFIR. Several types of examinations have been conducted to evaluate fission gas release, visual appearance, gamma emitting fission product content, chemical content, and microstructure. Overall, the irradiated UN kernels and UN TRISO kernels have performed quite well at this low burnup. The results

from fission gas release are mixed. As expected, no fission gas release was seen in the capsule that contained the TRISO-coated kernels. Some release that is generally in line with recoil release was observed in Capsules 222 and 223. Further investigation of the fission gas release observed for Capsules 221, 224, and 225 is still needed to understand the low Kr-85 activity observed for these capsules. The capsule disassembly demonstrated that it was possible to remove the particles from the Mo cups and that pre-irradiation particle identities can be retained, although there is room to improve this process. The microstructural examination of these kernels revealed good performance for these irradiation conditions. Very minimal irradiation-induced changes can be observed in the microstructure. These positive results justify continuing ongoing irradiations of UN kernels and UN TRISO to higher burnups (~6% FIMA), and they demonstrate how the MiniFuel design can be used for screening novel fuel concepts.

Acknowledgments

Several ORNL staff members contributed to the collection of the data discussed in this work. Mass spectrometry on the fuel was performed by Tamara Keever and Benjamin Roach. The hot-cell staff at the Irradiated Fuel Examination Laboratory, including Zachary Burns, Tyson Jordan, and Chuck Baldwin, were instrumental in data collection. Special recognition for the support of this experiment also goes to Annabelle LeCoq, Kory Linton, and Alicia Raftery. Andrew Nelson and Tyler Gerczak provided valuable comments on the manuscript. The work was supported by the Advanced Fuels Campaign of the United States Department of Energy (DOE) Office of Nuclear Energy. A portion of this research used resources at HFIR, a DOE Office of Science User Facility operated by ORNL.

References

[1] D.C. Crawford, D.L. Porter, S.L. Hayes, M.K. Meyer, D.A. Petti, K. Pasamehmetoglu, An Approach to Fuel Development and Qualification, *J. Nucl. Mater.* 371 (2007) 232–242. doi:10.1016/J.JNUCMAT.2007.05.029.

[2] C.M. Petrie, J.R. Burns, A.M. Raftery, A.T. Nelson, K.A. Terrani, Separate Effects Irradiation Testing of Miniature Fuel Specimens, *J. Nucl. Mater.* 526 (2019) 151783. doi:10.1016/j.jnucmat.2019.151783.

[3] K.A. Terrani, B.C. Jolly, J.M. Harp, Uranium Nitride Tristructural-Isotropic Fuel Particle, *J. Nucl. Mater.* 531 (2020) 152034. doi:10.1016/J.JNUCMAT.2020.152034.

[4] D.A. Petti, B.P. Collin, D. Marshall, A Summary of the Results from the DOE Advanced Gas Reactor (AGR) Fuel Development and Qualification Program, Idaho Natl. Lab. Rep. (2017) INL/EXT-16-40784. doi:10.2172/1369357.

[5] P.A. Demkowicz, J.D. Hunn, S.A. Ploger, R.N. Morris, C.A. Baldwin, J.M. Harp, P.L. Winston, T.J. Gerczak, I.J. van Rooyen, F.C. Montgomery, C.M. Silva, Irradiation Performance of AGR-1 High Temperature Reactor Fuel, *Nucl. Eng. Des.* 306 (2016) 2–13. doi:10.1016/J.NUCENGDES.2015.09.011.

[6] J.D. Hunn, C.A. Baldwin, F.C. Montgomery, T.J. Gerczak, R.N. Morris, G.W. Helmreich, P.A. Demkowicz, J.M. Harp, J.D. Stempien, Initial Examination of Fuel Compacts and TRISO Particles From the US AGR-2 Irradiation test, *Nucl. Eng. Des.* 329 (2018) 89–101. doi:10.1016/j.nucengdes.2017.09.017.

[7] C.A. Baldwin, J.D. Hunn, R.N. Morris, F.C. Montgomery, C.M. Silva, P.A. Demkowicz, First Elevated-Temperature Performance Testing of Coated Particle Fuel Compacts from the AGR-1 Irradiation Experiment, *Nucl. Eng. Des.* 271 (2014) 131–141. doi:10.1016/j.nucengdes.2013.11.021.

[8] R.N. Morris, J.D. Hunn, C.A. Baldwin, F.C. Montgomery, T.J. Gerczak, P.A. Demkowicz, Initial Results from Safety Testing of US AGR-2 Irradiation Test Fuel, *Nucl. Eng. Des.* 329 (2018) 124–133. doi:10.1016/j.nucengdes.2017.08.006.

[9] R.N. Morris, C.A. Baldwin, P.A. Demkowicz, J.D. Hunn, E.L. Reber, Performance of AGR-1 High-Temperature Reactor Fuel during Post-Irradiation Heating Tests, *Nucl. Eng. Des.* 306 (2016) 24–35. doi:10.1016/J.NUCENGDES.2016.04.031.

[10] Y. Arai, Nitride Fuel, *Compr. Nucl. Mater.* (2012) 41–54. doi:10.1016/B978-0-08-056033-5.00050-1.

[11] J.B.T.-R.M. in M.S. and M.E. Wallenius, Nitride Fuels☆, in: Elsevier, 2019. doi:https://doi.org/10.1016/B978-0-12-803581-8.11694-7.

[12] B. Hilton, D. Porter, S. Hayes, AFC-1 Transmutation Fuels Post-Irradiation Hot Cell Examination 4-8 at.% - Final Report (Irradiation Experiments AFC-1B, -1F and -1Æ), Idaho Natl. Lab. Rep. (2006) INL/EXT-05-00785. doi:10.2172/911779.

[13] J.M. Harp, S.L. Hayes, P.G. Medvedev, D.L. Porter, L. Capriotti, Testing Fast Reactor Fuels in a Thermal Reactor: A Comparison Report, Idaho Natl. Lab. Rep. (2017) INL/EXT-17-41677. doi:10.2172/1458766.

[14] C.M. Petrie, J.R. Burns, R.N. Morris, K.R. Smith, A.G. Le Coq, K.A. Terrani, Irradiation of Miniature Fuel Specimens in the High Flux Isotope Reactor, Oak Ridge Natl. Lab. Rep. (2018) ORNL/SR-2018/874. doi:10.2172/1458354.

[15] J.W. McMurray, R.D. Hunt, C.M. Silva, G.W. Helmreich, R.L. Seibert, Production of UN Kernels with Gd Additive as Burnable Absorber, Oak Ridge Natl. Lab. Rep. (2018) ORNL/SPR-2018/27 Rev. 1.

[16] J.W. McMurray, Fuel Material Certification Document Memo, McMurray to Petrie (2018).

[17] B. Jolly, G. Helmreich, J. Dyer, K.A. Terrani, Fabrication and Characterization of DU and LEU UN TRISO Particles, Oak Ridge Natl. Lab. Rep. (2016) ORNL/LTR-2016/384.

[18] J.W. McMurray, R.D. Hunt, T.J. Reif, G.W. Helmreich, C.M. Silva, R.L. Seibert, T.J. Gerczak, K.A. Terrani, Investigation of Sol-Gel Feedstock Additions and Process Variables on the Density and Microstructure of UN Microspheres, *J. Nucl. Mater.* 520 (2019) 78–86. doi:10.1016/j.jnucmat.2019.04.003.

[19] A.M. Raftery, R.N. Morris, K.R. Smith, G.W. Helmreich, C.M. Petrie, K.A. Terrani, A.T. Nelson, Development of a Characterization Methodology for Post-Irradiation Examination of Miniature Fuel Specimens, Oak Ridge Natl. Lab. Rep. (2018) ORNL/SPR-2018/918. doi:10.2172/1474563.

[20] J.M. Harp, P.A. Demkowicz, P.L. Winston, J.W. Sterbentz, An Analysis of Nuclear Fuel Burnup in the AGR-1 TRISO Fuel Experiment Using Gamma Spectrometry, Mass Spectrometry, and Computational Simulation Techniques, *Nucl. Eng. Des.* 278 (2014) 395–405. doi:10.1016/J.NUCENGDES.2014.07.041.

[21] A.A. Campbell, W.D. Porter, Y. Katoh, L.L. Snead, Method for Analyzing Passive Silicon Carbide Thermometry with a Continuous Dilatometer to Determine Irradiation Temperature, *Nucl. Instruments Methods Phys. Res. Sect. B Beam Interact. with Mater. Atoms.* 370 (2016) 49–58. doi:10.1016/J.NIMB.2016.01.005.

[22] W.J. Maeck, R.P. Larsen, J.E. Rein, Burnup Determination for Fast Reactor Fuels: A Review and Status of the Nuclear Data and Analytical Chemistry Methodology Requirements, US At. Energy Comm. TID-26209 (1973).

[23] K. Tanaka, K. Maeda, K. Katsuyama, M. Inoue, T. Iwai, Y. Arai, Fission Gas Release and Swelling in Uranium–Plutonium Mixed Nitride Fuels, *J. Nucl. Mater.* 327 (2004) 77–87. doi:https://doi.org/10.1016/j.jnucmat.2004.01.002.

[24] B.J. Lewis, Fission Product Release from Nuclear Fuel by Recoil and Knockout, *J. Nucl. Mater.* 148 (1987) 28–42. doi:https://doi.org/10.1016/0022-3115(87)90515-0.

[25] P.A. Demkowicz, J.D. Hunn, R.N. Morris, I.J. van Rooyen, T.J. Gerczak, J.M. Harp, S.A. Ploger, AGR-1 Post Irradiation Examination Final Report, Idaho Natl. Lab. Rep. (2015) INL/EXT-15-36407. doi:10.2172/1236801.

[26] I.J. Van Rooyen, T.M. Lillo, H. Wen, K.E. Wright, J.W. Madden, J.A. Aguiar, Advanced Electron Microscopy and Micro Analytical Technique Development And Application for Irradiated TRISO Coated Particles from the AGR-1 Experiment, Idaho Natl. Lab. Rep. (2017) INL/EXT-15-36281.

doi:10.2172/1364087.

[27] J.D. Hunn, R.N. Morris, C.A. Baldwin, F.C. Montgomery, G.W.C. Silva, AGR-1 Irradiated Compact 6-1-1 PIE Report: Evaluation of As-Irradiated Fuel Performance Using Leach Burn Leach, IMGA, Materialography, and X-ray Tomography, Oak Ridge Natl. Lab. Rep. (2012) ORNL/TM-2012/233 rev.0.

[28] J.D. Hunn, R.N. Morris, C.A. Baldwin, F.C. Montgomery, G.W.C. Silva, AGR-1 Irradiated Compact 4-4-2 PIE Report : Evaluation of As-Irradiated Fuel Performance with Leach Burn Leach, IMGA , Materialography , and X-ray Tomography, Oak Ridge Natl. Lab. Rep. (2013) ORNL/TM-2013/236.

[29] J.D. Hunn, T.J. Gerczak, F.C. Montgomery, D.J. Skitt, C.A. Baldwin, G.W. Helmreich, B.D. Eckhart, J.A. Dyer, AGR-2 As-Irradiated UCO Compact 5-4-2 PIE Report, Oak Ridge Natl. Lab. Rep. (2018) ORNL/TM-2018/863. doi:10.2172/1454396.